magnetochemistry

MDPI

Article

Magnetic and Luminescence Properties of 8-Coordinated Pyridyl Adducts of Samarium(III) Complexes Containing 4,4,4-Trifluoro-1-(naphthalen-2-yl)-1,3-butanedionate

Franz A. Mautner [1,*], Florian Bierbaumer [1], Ramon Vicente [2], Saskia Speed [2], Ánnia Tubau [2], Roland C. Fischer [3] and Salah S. Massoud [4,5,*]

[1] Institute of Physical and Theoretical Chemistry, Graz University of Technology, Stremayrgasse 9, A-8010 Graz, Austria; bierbaumerflorian97@gmail.com
[2] Departament de Química Inorgànica i Orgànica, Universitat de Barcelona, Martí i Franquès 1-11, E-08028 Barcelona, Spain; rvicente@ub.edu (R.V.); saskia.speed@qi.ub.es (S.S.); anniatubau@ub.edu (Á.T.)
[3] Institute of Inorganic Chemistry, Graz University of Technology, Stremayrgasse 9, A-8010 Graz, Austria; roland.fischer@tugraz.at
[4] Department of Chemistry, University of Louisiana at Lafayette, P.O. Box 43700, Lafayette, LA 70504, USA
[5] Department of Chemistry, Faculty of Sciences, Alexandria University, Moharam Bey, Alexandria 21511, Egypt
* Correspondence: mautner@tugraz.at (F.A.M.); ssmassoud@louisiana.edu (S.S.M.); Tel.: +43-316-873-32270 (F.A.M.); +1-337-482-5672 (S.S.M.); Fax: +43-316-873-8225 (F.A.M.); +1-337-482-5672 (S.S.M.)

Abstract: A novel series of polypyridyl adducts, [Sm(ntfa)$_3$(NN)] (**2**–**4**), with ntfa = 4,4,4-trifluoro-1-(naphthalen-2-yl)-1,3-butanedionate, NN = 2,2′-bipyridine (bipy), 4,4′-dimethyl-2,2′-bipyridine (4,4′-Me$_2$bipy), and 5,5′-dimethyl-2,2′-bipyridine (5,5′-Me$_2$bipy) were synthesized from the precursor complex [Sm(ntfa)$_3$(MeOH)$_2$] (**1**) and the corresponding pyridyl ligands. Single X-ray crystallography showed that the complexes displayed 8-coordinated geometry. The solid pyridyl adducts **2**–**4** exhibited emission of luminescence in the NIR and visible regions with close quantum yields (QY = 0.20–0.25%). The magnetic data of **1**–**4** showed larger values than those expected for magnetically noncoupled Sm(III) complexes in the $^6H_{5/2}$ ground state, with no saturation on the applied high magnetic field static at a temperature of 2 K.

Keywords: lanthanides; samarium; X-ray; diketones; magnetic properties; luminescence

Citation: Mautner, F.A.; Bierbaumer, F.; Vicente, R.; Speed, S.; Tubau, Á.; Fischer, R.C.; Massoud, S.S. Magnetic and Luminescence Properties of 8-Coordinated Pyridyl Adducts of Samarium(III) Complexes Containing 4,4,4-Trifluoro-1-(naphthalen-2-yl)-1,3-butanedionate. *Magnetochemistry* **2022**, *8*, 72. https://doi.org/10.3390/magnetochemistry8070072

Academic Editor: Manuel Almeida

Received: 28 January 2022
Accepted: 5 July 2022
Published: 11 July 2022

1. Introduction

Samarium-based compounds and metal–organic nanoparticles are interesting lanthanide emitters, especially in the NIR (700–1000 nm region), where the majority of the samarium(III) compounds exhibit orange/red light emission [1–9], but other lights are rare [9–12]. Many of these compounds have been widely used in biomedical fields in fluorescence imaging [13–16]. Other applications include Sm(III) complexes bound to β-diketones such as tris(4,4,4-trifluoro-1-phenyl-1,3-butanedionate) (btfa anion) and tris(4,4,4-trifluoro-1-(2-naphthyl)-1,3-butanedionate) (ntfa anion), which were further coordinated with auxiliary ligands such as 1,10-phenanthroline, and phosphine oxide derivatives were found to serve as luminescent probes for monitoring the progress of photopolymerization processes and the thickness of polymer coatings using the fluorescence probe technique (FPT) [17]. Recently, similar Sm(III)-β-diketonate complexes containing polypyridyl compounds were shown to exhibit white-light emission with reversible luminescence on/off switching properties, which increase their applications as sensors, display devices, biomarkers, and switches [18]. In addition, visible and near-infrared (NIR) emissions with high-luminescence quantum yields were observed in some related samarium(III)-β-diketonate complexes in ionic liquid mixtures [12,19].

According to the HSAB concept, lanthanide cations (Ln^{3+}) are classified as hard Lewis acids, and as a result, they exhibit strong binding affinity for hard Lewis bases including those containing *O*-donor ligands such as β-diketone compounds, where tris(β-diketonate) species are most likely formed [20–33]. The resulting complexes show a high tendency to expand their coordination numbers (CNs) from 6 to 9, and in some cases up to 12, through further interaction with various solvent molecules and/or auxiliary ligands such as hetero-atomic molecules [26–36], where the resulting coordinated β-diketonates act as efficient "antenna ligands" for lanthanides emitting in the UV, visible, and NIR region [21–42]. It has been stated that luminescence efficiency of the β-diketonate complexes can be enhanced by the appropriate choice of the Ln^{3+} ion and a combination of aromatic and fluorinated alkyl groups into the β-diketone ligands. This may lead to tuning the position of the ligands' triplet levels to result in good energy transfer between the diketonate ligands and the lanthanide ion [43–45] through reducing nonradiative quenching of lanthanide luminescence [43–49]. In addition, in some cases this approach may produce interesting double-functionality compounds of good luminescence emission in the visible and NIR regions and single-molecule magnet (SMM) behavior, as was observed in [Nd(ntfa)$_3$(NN)] complexes, where NN = phen, 5,5′-Me_2bipy and 4,4′-Mt_2bipy (4,4′-Mt_2bipy = 4,4′-dimethoxy-bipyridine) [32].

Following all the above, and in a continuous effort to explore the luminescence and magnetic properties of [Ln(β-diketonate)$_3$(NN)] pyridyl adducts [29–33] with the hope of designing intense luminescent molecules [21–42] that may exhibit slow relaxation of magnetization behavior [23–25,32,34,39,50], the high tendency of samarium(III) fluorinated β-diketonate compounds as good luminescent emitters in the visible and NIR regions [12,51] allowed us to synthesize and structurally characterize a novel series of polypyridyl adducts of Sm(III)-based 4,4,4-trifluoro-1-(naphthalen-2-yl)-1,3-butanedionate and study the luminescence emission and magnetic properties of the synthesized complexes.

2. Experimental

2.1. Materials and Physical Measurements

4,4,4-Trifluoro-1-(naphthalen-2-yl)-butane-1,3-dione, 2,2′-bipyridine, 4,4′-dimethyl-2,2′-bipyridine, and 5,5′-dimethyl-2,2′-bipyridine were purchased from TCI, Sm(NO$_3$)$_3$.6H$_2$O was purchased from Sigma Aldrich, and the other chemicals were of analytical-grade quality. Infrared spectra of solid complexes were recorded on a Bruker Alpha P (platinum-ATR-cap) spectrometer (Bruker AXS, Madison, WI, USA). PXRD patterns were recorded with a Bruker D8 Advance powder diffractometer (Cu-Kα radiation) (Bruker AXS, Madison, WI, USA) and full-pattern profile fits were performed (Highscore Plus, Panalytical, The Netherlands) [52]. Elemental microanalyses were carried out with an Elementar Vario EN3 analyzer (Langenselbold, Germany). The magnetic susceptibility and magnetization measurements were performed at the Magnetic Measurements Unit of the University of Barcelona using the Quantum Design MPMS-XL SQUID magnetometer. Diamagnetic corrections were estimated with the aid of Pascal's constants [53], and were subtracted from the experimental susceptibilities to give the corrected molar magnetic susceptibilities.

2.2. X-ray Crystal Structure Analysis

A Bruker-AXS APEX CCD single-crystal X-ray diffractometer (Bruker-AXS; Madison, WI, USA) with Mo-Kα radiation (λ = 0.71073 Å) and equipped with an Oxford Cryostream 700 cooling system was used for data collection at 100(2) K. Crystallographic data of the four title complexes are summarized in Table 1. SADABS and APEX computer programs [54,55] for absorption corrections and data processing were applied. The SHELX program package [56,57] was used for structure solution and refinement (direct methods, F^2 based full-matrix least-squares). The programs Mercury [58] and Platon [59] also were used. Partial disorder was observed in one -CF_3 group of **2**. CCDC 1,964,549–CCDC 1,964,553 contained the crystallographic data in CIF format for **1**–**4**, respectively.

Table 1. Crystallographic data and processing parameters for **1**–**4**.

Compound	**1**	**2**	**3**	**4**
Empirical formula	$C_{44}H_{32}F_9O_8Sm$	$C_{52}H_{32}F_9N_2O_6Sm$	$C_{54}H_{36}F_9N_2O_6Sm$	$C_{54}H_{36}F_9N_2O_6Sm$
Formula mass	1010.06	1102.16	1130.21	1130.21
System	Monoclinic	Monoclinic	Monoclinic	Orthorhombic
Space group	$P2_1/c$	$P2_1/c$	$P2_1/n$	$Pca2_1$
a (Å)	8.9705(6)	11.1681(6)	11.4354(5)	20.1759(10)
b (Å)	28.9157(19)	23.2377(13)	27.7564(11)	11.8320(6)
c (Å)	16.1596(10)	17.8086(9)	15.2341(6)	19.6052(9)
α (°)	90	90	90	90
β (°)	105.656(3)	97.051(3)	104.582(2)	90
γ (°)	90	90	90	90
V (Å3)	4036.1(5)	4586.8(4)	4679.6(3)	4680.2(4)
Z	4	4	4	4
T (K)	100(2)	100(2)	100(2)	100(2)
μ (mm^{-1})	1.551	1.371	1.346	1.345
Dcalc (Mg/m^3)	1.662	1.596	1.604	1.604
θ max (°)	30.000	26.998	27.880	27.993
Data collected	310,348	101,889	71,436	124,790
Unique refl./Rint	11,773/0.0353	10,015/0.0684	11,132/0.0525	11,059/0.0745
Parameters/Restraints	567/0	631/0	670/24	651/1
Goodness-of-Fit on F^2	1.176	1.031	1.177	1.016
R1/wR2 (all data)	0.0370/0.0689	0.0447/0.0779	0.0469/0.0914	0.0371/0.0739

2.3. Fluorescence Measurements

Solid-state fluorescence spectra of the title compounds **1**–**4** were recorded on a Horiba Jobin Yvon SPEX Nanolog fluorescence spectrophotometer (Fluorolog-3 v3.2, HORIBA Jovin Yvon, Cedex, France), which was equipped with a three-slit double-grating excitation and emission monochromator with dispersions of 2.1 nm/mm (1200 grooves/mm) at room temperature. The steady-state luminescence of the solid samples was excited by unpolarized light from a 450 W xenon CW lamp and detected at an angle of 22.5° by a red-sensitive Hamamatsu R928 photomultiplier tube. Spectral corrections were made for both the emission spectral response (detector and grating) and the excitation source light-intensity variation (lamp and grating). NIR spectra (800–1400 nm) were recorded at an angle of 22.5° using a solid InGaAs detector and liquid nitrogen as a coolant. The lifetime excited state (τ_{obs}) of the $^4G_{5/2}$ emissions was measured on the same instrument in the phosphorescence mode using a 450 W xenon pulsed lamp (1.5 ns pulse), and the measured decays were analyzed using the Origin software package. The decay curves of the compounds **1**–**4** were fitted monoexponentially with Equation (1):

$$I(t) = I_0 \exp\left(-\frac{t}{obs}\right) \quad (1)$$

The Pearson Chi^2 method was used to determine the fit quality. Absolute quantum yield (Φ_{TOT}) measurements were acquired in the G8 Quantum Integrating Sphere from

GMP engaged with an interior reflective coating (Spectralon®). The Φ_{TOT} was calculated using Equation (2):

$$\Phi = \frac{E_c - E_c(blank)}{L_a - L_c} \quad (2)$$

where L_c is the calculated area of the outgoing amount of light after interaction with the sample, and L_a is the calculated area without interaction with the sample (*blank*) at the λ_{exc} and E_c referees to the calculated area from the emission spectrum of the sample and E_c (*blank*) from the corresponding spectrum of the *blank*.

2.4. Synthesis of the Complexes

2.4.1. $[Sm(ntfa)_3(MeOH)_2]$ (**1**)

$Sm(NO_3)_3{\cdot}6H_2O$ (444 mg, 1 mmol) dissolved in MeOH (10 mL) was added to a methanol solution (15 mL) containing NaOH (3 mmol, 0.120 g) and Hntfa (1 mmol, 799 mg). This solution was stirred for 2 h at room temperature, then 10 mL of deionized water was added to the reaction mixture and stirred at 50 °C for another 6 h. The resulting solution was filtered through celite and then allowed to crystallize at room temperature. On the following day, the well-shaped shiny yellow crystals were filtered and dried in air (overall yield: 886 mg, 88%). Anal. Calcd. for $C_{44}H_{32}F_9O_8Sm$ (1010.066 g/mol): C, 52.32; H, 3.19%. Found: C, 52.33; H, 3.32%. Selected IR bands (ATR-IR, cm^{-1}): 3410 (vw, br), 1607 (s), 1568 (m), 1530 (m), 1507 (m), 1457 (m), 1431 (m), 1353 (w), 1288 (m), 1251 (m), 1182 (m), 1124 (vs), 1076 (m), 984 (m), 956 (m), 863 (m), 795 (vs), 759 (m), 682 (s).

2.4.2. $[Sm(ntfa)_3(bipy)]$ (**2**)

$[Sm(ntfa)_3(MeOH)_2]$ (211 mg, 0.21 mmol) was dissolved in 15 mL ethanol/acetone (4:1), and 2,2′-bipyridyl (36 mg, 0.23 mmol) was dissolved in 15 mL ethanol/acetone (4:1). The solutions were combined and stirred for 2 h. The reaction mixture was filtered and allowed to crystallize at room temperature. After seven days, the yellow crystals, which were separated, were collected by filtration and dried in air (yield: 149 mg, 64%). Anal. Calcd. for $C_{52}H_{32}F_9N_2O_6Sm$ (1102.16 g/mol): C, 56.67; H, 2.93; N, 2.54%. Found: C, 56.49; H, 2.84; N, 2.68%. Selected IR bands (ATR-IR, cm^{-1}): 1609 (s), 1589 (m), 1567 (m), 1529 (m), 1508 (m), 1460 (m), 1435 (w), 1385 (w), 1355 (w), 1286 (s), 1182 (m), 1129 (s), 1072 (w), 1013 (m), 955 (m), 927 (w), 867 (w), 822 (w), 791 (s), 760 (s), 681 (s), 644 (w), 566 (m), 518 (w), 467 (m), 404 (w).

2.4.3. $[Sm(ntfa)_3(4,4'\text{-}Me_2bipy)]$ (**3**)

$[Sm(ntfa)_3(MeOH)_2]$ (109 mg, 0.11 mmol) and 4,4′-dimethyl-2,2′-dipyridyl (37 mg, 0.20 mmol) were dissolved in 30 mL ethanol/acetone (2:1). The solution was stirred for approximately for 2 h. The mixture was filtered and allowed to crystallize at room temperature. After seven days the yellow crystals, which were separated, were collected by filtration and dried in air (yield: 60 mg, 48%). Anal. Calcd. for $C_{54}H_{36}F_9N_2O_6Sm$ (1130.21 g/mol): C, 57.39; H, 3.21; N, 2.48%. Found: C, 57.61; H, 3.32; N, 2.39%. Selected IR bands (ATR-IR, cm^{-1}): 1606 (s), 1590 (m), 1568 (m), 1526 (m), 1506 (m), 1474 (w), 1385 (w), 1353 (w), 1287 (s), 1219 (w), 1185 (m), 1132 (s), 1073 (w), 956 (m), 911 (w), 863 (w), 792 (s), 751 (m), 680 (m), 566 (m), 517 (w), 468 (m).

2.4.4. $[Sm(ntfa)_3(5,5'\text{-}Me_2bipy)]$ (**4**)

$[Sm(ntfa)_3(MeOH)_2]$ (238 mg, 0.24 mmol) was dissolved in 15 mL ethanol/acetone (4:1), and 5,5′-dimethyl-2,2′-dipyridyl (48 mg, 0.26 mmol) was dissolved in 15 mL ethanol/acetone (4:1). The solutions were combined and stirred approximately for 2 h. The reaction mixture was filtered and left to crystallize at room temperature. After 10 days the yellow crystals, which were separated, were collected by filtration and dried in air (yield: 157 mg, 58%). Anal. Calcd. for $C_{54}H_{36}F_9N_2O_6Sm$ (1130.21 g/mol): C, 57.39; H, 3.21; N, 2.48%. Found:

C, 57.54; H, 3.14; N, 2.57%. Selected IR bands (ATR-IR, cm^{-1}):1607 (s), 1589 (m), 1566 (m), 1526 (m), 1506 (m), 1475 (w), 1384 (w), 1353 (w), 1287 (s), 1218 (w), 1182 (m), 1132 (s), 1073 (w), 956 (m), 935 (w), 863 (w), 791 (s), 751 (m), 680 (m), 566 (m), 517 (w), 468 (m), 414 (w).

3. Results and Discussion

3.1. Synthetic Aspects and IR Spectra of the Complexes

The yellow crystalline complex [Sm(ntfa)$_3$(MeOH)$_2$] (**1**) was obtained at an 88% yield. The synthesis was straightforward, and conducted by stirring a methanolic solution containing Sm(NO$_3$)$_3$·6H$_2$O, 4,4,4-trifluoro-1-(naphthalen-2-yl)-butane-1,3-dione (Hntfa), and NaOH in a stochiometric ratio of 1:3:3, followed by the addition of H$_2$O and stirring for 6 h at 50 °C. The complex [Sm(ntfa)$_3$(MeOH)$_2$] (**1**) was used as the precursor for the synthesis of the yellow crystalline polypyridyl adducts [Sm(ntfa)$_3$(NN)], where NN = bipy (**2**), 4,4′-Me$_2$bipy (**3**) and 5,5′-Me$_2$bipy (**4**) in EtOH-acetone mixtures in moderate yields (48–64%). This approach was successfully used for the synthesis of other similar monobipyridyl Ln(III) (Ln = La, Pr, Nd, and Ho) compounds containing β-diketonate derivatives [30–34]. The isolated complexes **1**–**4** were structurally characterized using elemental microanalyses, IR spectroscopy, and single-crystal X-ray crystallography. In addition, their purity was checked using PXRD powder diffraction (Supplementary Figures S1–S4 in the Supplementary Materials section).

The IR spectra of complexes **1**–**4** displayed general characteristic features, such as a strong vibrational band observed around 1608 ± 2 cm^{-1} that is typically assigned to the stretching frequency ν(C=O) of the coordinated carbonyl group of ntfa [47–49], as well as a series of medium intense bands over the frequency range of 1600–1506 cm^{-1}. In addition, complex **1** exhibited a weak broad band centered at 3410 cm^{-1} assigned to the ν(O-H) stretching frequency of the coordinated methanol ligands.

3.2. Description of the Crystal Structures

Partially labelled molecular plots of the title compounds **1**–**4** are presented in Figure 1, and coordination figures are depicted in Figure 2. In addition, the selected bond distances and bond angles of **1**–**4** are given in Table 2. Coordination number (CN) eight was observed around each Sm(III) center in the neutral monomeric complexes **1**–**4**. All metal centers were ligated by six oxygen-donor atoms of three β-diketonate ligand anions with Sm1-O(keto) bond distances in the range of 2.3388(18) to 2.4296(17) Å, and O-Sm1-O keto-bite angles ranging from 69.86(6) to 71.68(8)°. In **1,** the Sm1 center was further ligated by oxygen atoms of two terminal methanol molecules (Sm1-O7 = 2.5382(18), Sm1-O8 = 2.4487(18) Å). Coordination number 8 in compounds **2**–**4** was completed by two N atoms of chelating bipy or Me$_2$-bipy ligands with Sm1-N bond distances varying from 2.562(3) to 2.597(3) Å and with N1-Sm1-N2 chelate bite angles varying from 62.25(9) to 63.12(16)°.

The degree of distortion of the coordination polyhedra from their ideal polyhedron geometry were analyzed using the continuous shape measure theory with the SHAPE software [60,61]. Intermediate distortion from the ideal eight-vertex coordination polyhedra was observed for the LaO$_8$ in **1** and LaO$_6$N$_2$ coordination polyhedron of **2**–**4**. The lowest CShM values for compound **1** corresponded to a triangular dodecahedron (TDD-8), biaugmented trigonal prism (BTPR-8), square antiprism (SAPR-8), and biaugmented trigonal prism J50 (JBTPR-8), with values of 0.335, 1.652, 2.335, and 2.667, respectively. The following respective values were found: 1.239, 1.639, 1.262, and 2.197 in the case of **2**; 1.050, 2.494, 1.498, and 3.044 for **3;** and 2.258, 1.913, 0.696, and 2.453 for **4**. All these values are summarized in Table 3 for the four compounds.

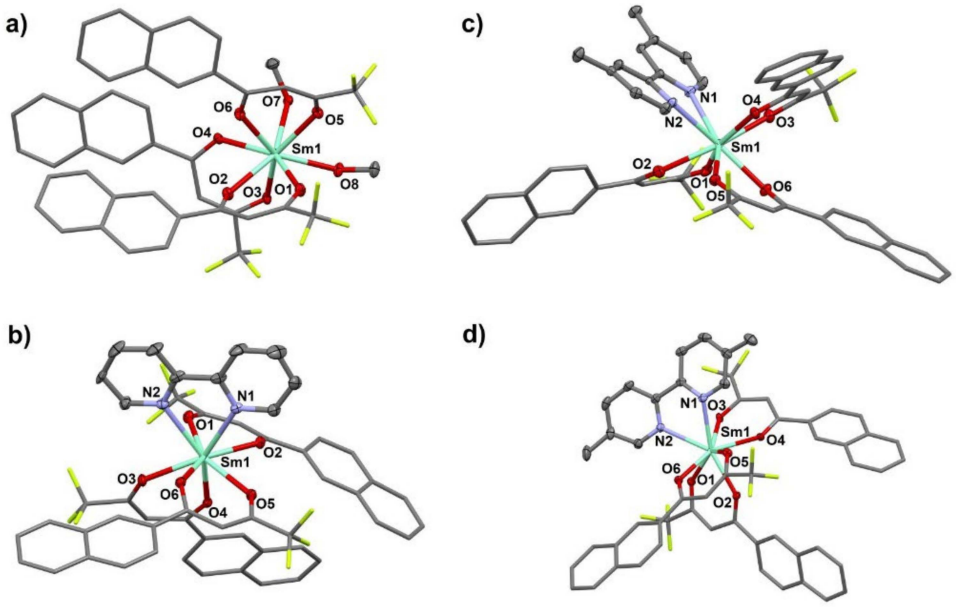

Figure 1. Partially labelled molecular plots of (**a**) [Sm(ntfa)$_3$(MeOH)$_2$] (**1**), (**b**) [Sm(ntfa)$_3$(bipy)] (**2**), (**c**) [Sm(ntfa)$_3$(4,4′-Me$_2$bipy)] (**3**), and (**d**) [Sm(ntfa)$_3$(5,5′-Me$_2$bipy)] (**4**). Color code: turquoise: Sm, red: oxygen, blue: nitrogen, black: carbon, and green: fluorine; H atoms omitted for clarity.

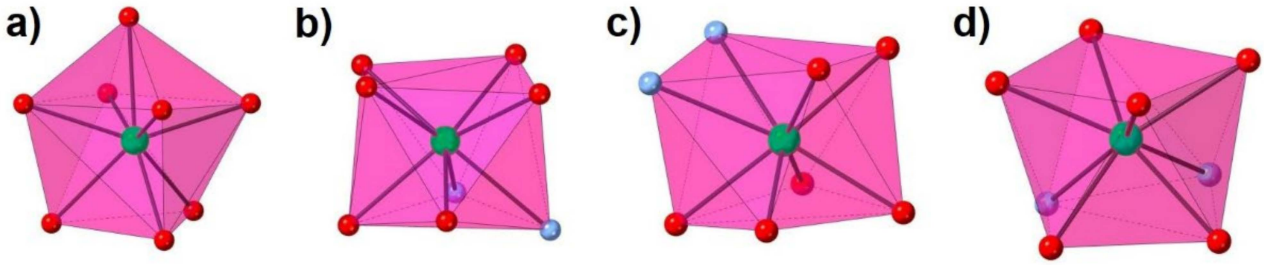

Figure 2. Coordination figures (**a**–**d**) of **1**–**4** compounds, respectively. Color code: turquoise: Sm, red: oxygen, and blue: nitrogen.

Table 2. Selected bond distances (Å) and bond angles (°) of **1**–**4**.

Compound	1	2	3	4
Sm1-O1	2.3697(18)	2.371(2)	2.387(2)	2.381(4)
Sm1-O2	2.3388(18)	2.393(2)	2.395(2)	2.367(4)
Sm1-O3	2.4296(17)	2.373(2)	2.386(2)	2.398(4)
Sm1-O4	2.4156(17)	2.355(2)	2.362(2)	2.346(4)
Sm1-O5	2.3615(18)	2.416(2)	2.379(2)	2.390(4)
Sm1-O6	2.3795(17)	2.360(2)	2.370(2)	2.372(4)
Sm1-N1		2.579(3)	2.562(3)	2.576(5)
Sm1-N2		2.597(3)	2.588(3)	2.576(5)
Sm1-O7	2.5382(18)			
Sm1-O8	2.4487(18)			
O1-Sm1-O2	70.65(6)	71.51(8)	70.20(9)	71.35(13)
O3-Sm1-O4	69.86(6)	71.06(8)	71.68(8)	70.44(13)
O5-Sm1-O6	71.49(6)	69.91(8)	71.10(8)	70.70(14)
N1-Sm1-N2		62.63(10)	62.25(9)	63.12(16)

Table 3. Lowest values of the calculated continuous shape measurements (CShMs) for compounds **1**–**4**.

Compound	Triangular Dodecahedron (TDD-8, D_{2d})	Biaugmented Trigonal Prism (BTPR-8, C_{2v})	Square Antiprism (SAPR-8, D_{4d})	Biaugmented Trigonal Prism J50 (JBTPR-8, C_{2v})
1	0.335	1.652	2.335	2.667
2	1.239	1.639	1.262	2.197
3	1.050	2.494	1.498	3.044
4	2.258	1.913	0.696	2.453

The packing plots of **1**–**4** are presented in Supplementary Figures S5–S8 in the Supplementary Materials section. The O-H groups of the two methanol molecules in **1** formed hydrogen bonds of type O-H···O (O7···O3(-x,-y,-z) = 2.713(2) Å; O7-H10···O3(-x,-y,-z) = 158(3)°; O8···O7(-x,-y,-z) = 2.740(3) Å; O8-H20···O7(-x,-y,-z) = 162(4)°) (Supplementary Figure S5). The aromatic naphthyl- (in **1**–**4**) and pyridyl- (in **2**–**4**) moieties were involved in numerous ring···ring and C-H/F···ring interactions, which further stabilized the packing of the mononuclear complexes (Supplementary Tables S1–S4).

3.3. Photoluminescent Properties

The UV–visible excitation spectra of solid samples of the complexes **1**–**4** represented in Supplementary Figure S9 show a slight redshift of the intense broad band over the 350–400 nm region, which may be taken as an indication of the complex formation. These bands located at 400, 394, 392, and 389 nm for **1**–**4**, respectively, corresponded to $\pi \rightarrow \pi^*$ electronic transition in the conjugated ligands coordinated to the central samarium(III) ion. Excitation of the solid sample at these wavelengths (λ_{ex}) led to the Sm^{3+}-centered emission transitions in the visible and NIR regions.

The excitation and emission spectra of the compounds were recorded at room temperature in the visible and NIR regions and at the liquid nitrogen temperature (77 K) in the visible range; these spectra are shown in Figure 3 for the four complexes. Inspection of these spectra indicated an almost similar emission trend for all compounds. The bands in the visible region were assigned to $^4G_{5/2} \rightarrow {}^6H_{5/2}$ at 565 ± 1 nm, $^4G_{5/2} \rightarrow {}^6H_{7/2}$ at 608 ± 2 nm, and $^4G_{5/2} \rightarrow {}^6H_{9/2}$ at 649 ± 2 nm, while a less intense band at 714 ± 3 nm corresponded to the $^4G_{5/2} \rightarrow {}^6H_{11/2}$ transition. Additionally, the very-low-intensity band located at 535 nm could be discerned as the *f-f* transition from an upper emissive level to the ground state: $^4F_{3/2} \rightarrow {}^6H_{5/2}$ [12,62].

For compound **1**, the $^4F_{3/2} \rightarrow {}^6H_{5/2}$ transition at room temperature was not detected, and this probably could be attributed to the low-intensity residual emission from the ligand in the 450–500 nm range. For **2**–**4**, no emission from the ligand could be perceived, indicating a rather good energy transfer efficiency from the ligand's lowest triplet state to the resonant highest energy level of the Sm^{3+} ion. Moreover, the presence of a broad band from the absorption of the ligands in the excitation spectra suggested a good antenna effect [63]**.** The most intense band observed for the **1**–**4** compounds, which corresponded to the $^4G_{5/2} \rightarrow {}^6H_{9/2}$ transition, was a hypersensitive band (electric dipole allowed transition, $\Delta J = 2$) and due to its high intensity, it dominated in the final color that the compounds presented. Additionally, the $^4G_{5/2} \rightarrow {}^6H_{5/2}$ and $^4G_{5/2} \rightarrow {}^6H_{7/2}$ were magnetic dipole transitions ($\Delta J = 0, 1$ respectively), and the $^4G_{5/2} \rightarrow {}^6H_{9/2}/{}^4G_{5/2} \rightarrow {}^6H_{5/2}$ ratio provided information about the polarizability of the Sm^{3+} chemical environment. Ratio values of 6.25, 4.52, 4.62, and 4.17 were determined for compounds **1**–**4**, respectively. The similar ratio values observed in compounds **2**–**4** indicated that their coordination environment was not altered when the NN-donor ligand was changed. The higher ratio value detected in **1** indicated a more polarized environment around the Sm^{3+} ion, which obviously was attributed to the coordinated MeOH molecules [64]. The difference in the hypersensitive band intensity of **1**–**4** compounds was also perceived in the emission color, and could be

seen by naked eye under a UV lamp and according to the CIE diagram represented in Figure 4.

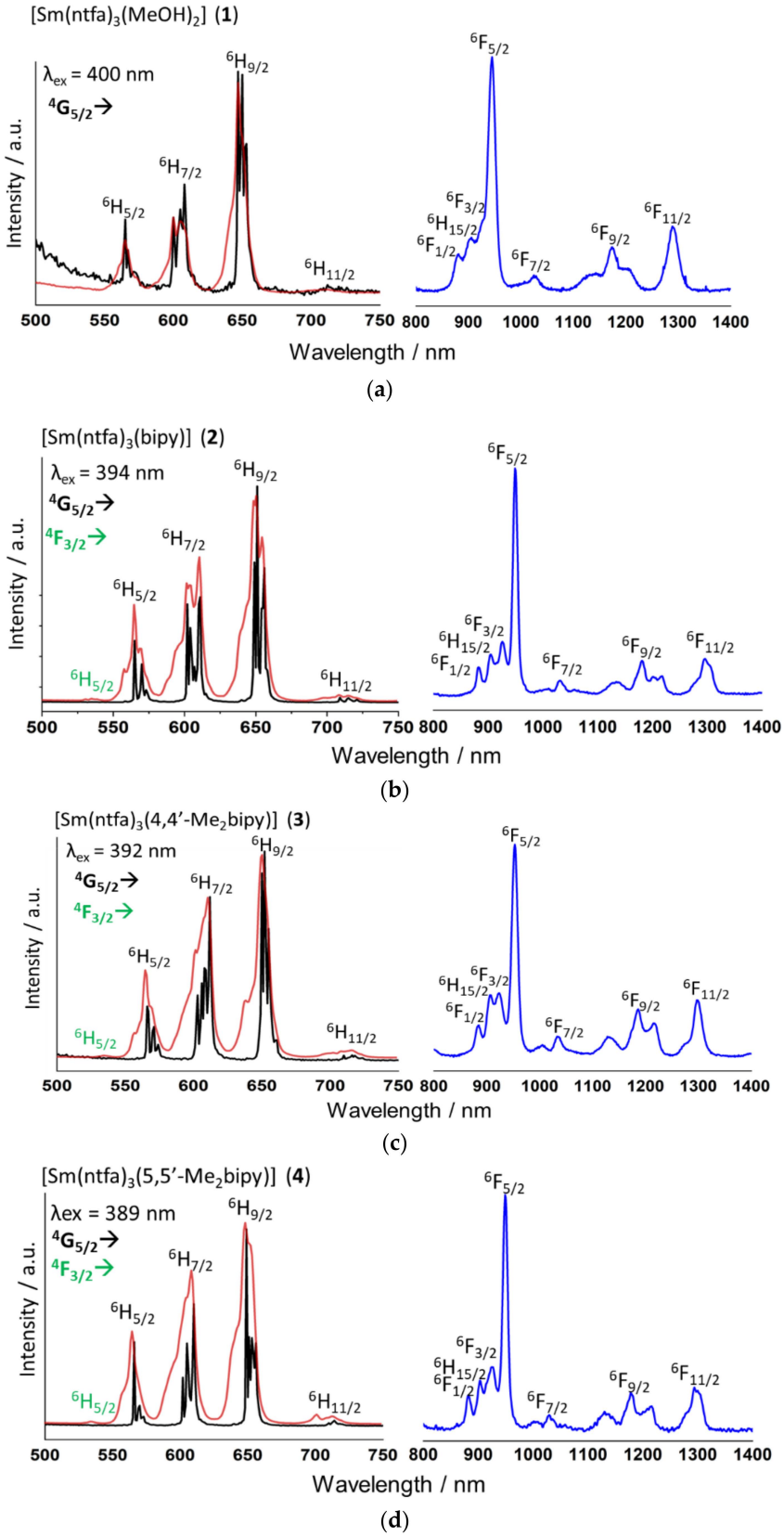

Figure 3. (**a**–**d**) The solid-state emission spectra of compounds **1**–**4** in the visible (red color at room temperature and black at 77 K) and NIR (blue color at 77 K) regions.

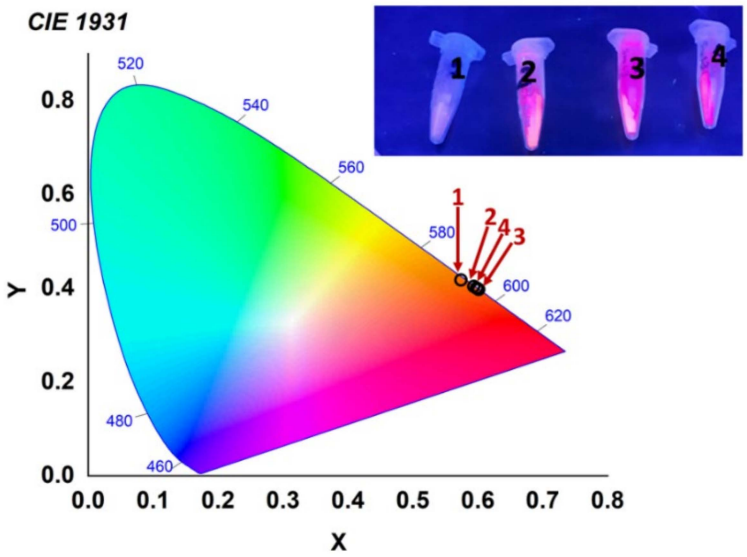

Figure 4. CIE diagram of the emission color of compounds **1–4**. Inset shows the emission of compounds under UV light.

The visible spectra of the compounds, which were also measured at the liquid nitrogen temperature (77 K), displayed the splitting of each band due to the crystal field perturbation, corresponding to the Stark sublevels of the Sm^{3+} Kramer ion. The ^6H_J energy levels of the four complexes should split to a maximum of $J + 1/2$ Stark according to symmetries lower than cubic for J half-integer values. Higher asymmetry around the Sm^{3+} ion is related to an enhancement of the emission intensity [2,21]. Thus, based on the results obtained in the SHAPE measurements, compounds **1–4** presented symmetries lower than cubic (O_h, O, T_d, T_h and T). Thus, it was expected that each band corresponding to different ^6H_J energy levels should split into three for $^6H_{5/2,}$ four for $^6H_{7/2}$, five for $^6H_{9/2}$, and six for $^6H_{11/2}$. However, if the symmetry around the Sm^{3+} ion was cubic, then the splitting due to the crystal field would be two, three, three, and four for each energy level, respectively [65,66]. The magnetic-dipole-allowed transition $^4G_{5/2} \rightarrow {}^6H_{7/2}$ was taken as a reference. For compounds, deconvolution of the $^4G_{5/2} \rightarrow {}^6H_{7/2}$ band was conducted, and the best fittings for the four compounds were performed when four Gaussian functions were used (Supplementary Figure S10), corroborating that the symmetry of the coordination polyhedron was lower than cubic. Moreover, the low-intensity transition $^4F_{3/2} \rightarrow {}^6H_{5/2}$ seen at 535 nm at room temperature measurements was not discerned at 77 K. The $^4F_{3/2}$ level, which was close in energy to the emitting $^4G_{5/2}$ level, was thermally populated at room temperature [52]. Furthermore, the $^4G_{5/2} \rightarrow {}^6H_{9/2}/{}^4G_{5/2} \rightarrow {}^6H_{5/2}$ intensity ratio was measured for the 77 K spectra. The obtained values were 6.29 for **1**, 4.55 for **2**, 4.66 for **3,** and 4.24 for **4**. These values were very similar to those obtained from the room temperature spectra, suggesting that there was no change in the coordination Sm^{3+} environment when the temperature changed.

The emission spectra of **1–4** enabled us to analyze the transition from the lowest emitting energy level to the ground state ($^4G_{5/2} \rightarrow {}^6H_J$) for each compound, and as can be seen in Figure 3, this emission presented five different bands that corresponded to the five expected levels for J = 5/2-13/2 centered at 565, 606, 647, 711, and 904 nm for **1**; at 564, 606, 649, 712, and 905 nm for **2**; at 565, 611, 651, 717, and 906 nm for **3;** and at 566, 610, 649, 714, and 903 nm for **4**. These transitions provided information about the crystal-field energy of the samarium ions in the complexes, and allowed us to estimate the energy between the ground ($^6H_{5/2}$) and first-excited ($^6H_{7/2}$) J states. The energy differences between these two transitions were about 1197, 1228, 1335, and 1275 cm^{-1} for the **1–4** complexes, respectively. The energy separation between the $^6H_{5/2}$ ground state of the samarium(III) and the first-excited state $^6H_{7/2}$ was evaluated as 1000 cm^{-1} [67], which was in good accordance with

the calculated values for **1–4.** From the energy separation between the first state $^6H_{7/2}$ and the $^6H_{5/2}$ ground state calculated previously from the emission spectra, we could evaluate the spin-orbit coupling parameter, λ, through the expression E(J) = λJ(J + 1)/2 [67]. These calculations led to λ values of 342, 351, 381, and 364 cm^{-1} for **1–4**, respectively.

Compounds **1–4** also showed Sm^{3+}-centered *f-f* emissions in the NIR region when exciting the samples at the corresponding λ_{ex} of the ligands. The experimental emission bands were from the $^4G_{5/2}$ emitting level to the ^6F_J energy level. These bands were assigned to $^4G_{5/2} \rightarrow {}^6F_{1/2}$ at 882 ± 1 nm; $^4G_{5/2} \rightarrow {}^6F_{3/2}$ at 925 ± 2 nm (in **1**, this band appeared as a shoulder); $^4G_{5/2} \rightarrow {}^6F_{5/2}$, which was the most intense band at 948 ± 3 nm; as well as the $^4G_{5/2} \rightarrow {}^6F_{7/2}$, $^4G_{5/2} \rightarrow {}^6F_{9/2}$, and $^4G_{5/2} \rightarrow {}^6F_{11/2}$ transitions at 1031 ± 5, 1180 ± 6, and 1294 ± 4 nm, respectively. In addition, the $^4G_{5/2} \rightarrow {}^6H_{15/2}$ transition was seen at 904 ± 1 nm [62,68–70]. All the bands arising from the *f-f* transitions of the Sm^{3+} ion (except for the $^4F_{3/2} \rightarrow {}^6H_{5/2}$ transition) came from the Sm^{3+} lowest emitting energy level, $^4G_{5/2}$. However, the $^4G_{5/2}$ was close in energy to the upper levels $^4G_{7/2}$ and $^4F_{3/2}$. These resulted in a fast nonradiative relaxation of the $^4G_{7/2}$ and $^4F_{3/2}$ to the $^4G_{5/2}$. Then, further radiative relaxation to the ^6F_J, in the NIR range, and to the ground state ^6H_J, in the visible range took place [63].

The luminescence quantum yield (QYs) in the solid state were determined using an integrating sphere. Only the visible emission range was determined. For **1**, the QY could not be calculated due to the low emission intensity that the sample presented, evidencing the effect of high-energy oscillators in the effectiveness of radiative deactivation. For **2**, **3,** and **4,** the close QY values were evaluated as 0.23, 0.25, and 0.20%, respectively.

Excited-state lifetimes (τ_{obs}) of the $^4G_{5/2}$ emitting state in the **1–4** complexes were collected at the maximum emission band in the visible range ($^4G_{5/2} \rightarrow {}^6H_{9/2}$, 649 ± 2 nm), where the decay curves were fitted monoexponentially as $\left(I(t) = I_0 \cdot \exp\left(-\frac{t}{\tau_{obs}}\right)\right)$ (Figure 5), according to single emitting species for all Sm^{3+} complexes. The measured τ_{obs} values were in the 30–74 μs range. The lowest value of τ_{obs} was obtained for the precursor compound. For compounds **2–4,** τ_{obs} increased when the NN-donor ligand was used, in the order: 5,5′-Me_2bipy < bipy < 4,4′-Me_2bipy. The same tendency was followed for the measured QYs. Compound **3** showed more luminescence intensity, suggesting an enhancement of the electron density around the Sm^{3+} ion due to the electron-donating methyl groups in the 4,4′ positions of the bipyridine ligand [69]. The photoluminescent data for QYs and τ_{obs} are compiled in Table 4.

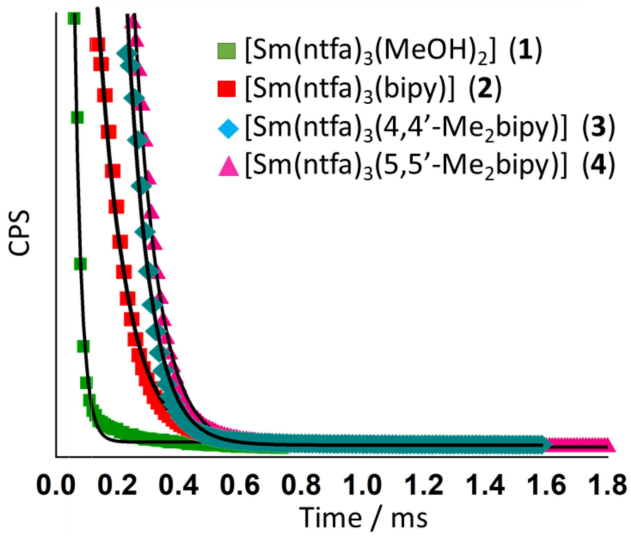

Figure 5. Photoluminescence time decay of compounds **1–4** monitored at the maximum emission wavelength of 649 ± 2 nm ($^4G_{5/2} \rightarrow {}^6H_{9/2}$). Solid lines represent the monoexponential fitting of the decay curves.

Table 4. Compilation of the photoluminescent data of compounds **1**–**4**. QY stands for the overall quantum yield, and τ_{obs} for the emission time delay.

Compound	$^4G_{5/2} \rightarrow {}^6H_{9/2}/{}^4G_{5/2} \rightarrow {}^6H_{5/2}$ Ratio	QY (%)	τ_{obs} (μs)
$[Sm(ntfa)_3(MeOH)_2]$ (**1**)	6.25	-	30
$[Sm(ntfa)_3(bipy)]$ (**2**)	4.52	0.23	74
$[Sm(ntfa)_3(4,4'\text{-}Me_2bipy)]$ (**3**)	4.62	0.25	80
$[Sm(ntfa)_3(5,5'\text{-}Me_2bipy)]$ (**4**)	4.17	0.20	65

In general, Sm^{3+} coordination compounds did not produce relatively high QYs because the energy gap between the lowest emitting sublevel $^5G_{5/2}$ and the lower energy level $^6F_{11/2}$ was 7500 cm^{-1}. This value was low compared to the energy difference from Tb^{3+} or Eu^{3+} ions, which were 12,500 cm^{-1} {ΔE ($^5D_0 \rightarrow {}^7F_6$)} and 14,800 cm^{-1} {ΔE ($^5D_4 \rightarrow {}^7F_6$)}, respectively. The small energy gap in Sm^{3+} ion favored nonradiative relaxation processes that lowered the emission efficiency and luminescence lifetimes. However, samarium(III) coordination compounds are very interesting due to their capability of emission over a wide range within the electromagnetic spectrum, thus covering both the visible and NIR regions [70–74]. The results obtained here were similar to those for other previously published samarium(III)-β-diketonate systems [2,63,65,70]

3.4. Magnetic Properties

DC Magnetic Susceptibility Studies

Powder samples of complexes **1**–**4** were measured under applied magnetic fields of 0.3 T (300–2 K). The data are plotted as $\chi_M T$ products versus T in Figure 6. Magnetization dependence of the applied field at 2 K for compounds were also recorded and are shown in Figure 7. The magnetic measurements of **1**–**4** revealed that the χ_MT values at 300 K were 0.35, 0.48, 0.35, and 0.29 $cm^3 \cdot mol^{-1} \cdot K$, respectively, which were larger than the theoretical value for a free Sm(III) ion (0.09 $cm^3 \cdot mol^{-1} \cdot K$) in the $^6H_{5/2}$ ground state ($g_J = 2/7$) [75], but in accordance with the room temperature χ_MT values of previously reported Sm(III) complexes [76–78]. Upon cooling the samples, the χ_MT values decreased practically linearly, reaching values of 0.04, 0.03, 0.04, and 0.03 $cm^3 \cdot mol^{-1} \cdot K$ for compounds **1**–**4**, respectively. These relatively small low temperature χ_MT values found in the compounds could be attributed to the significant crystal field (CF) splitting under an anisotropic coordination environment [78].

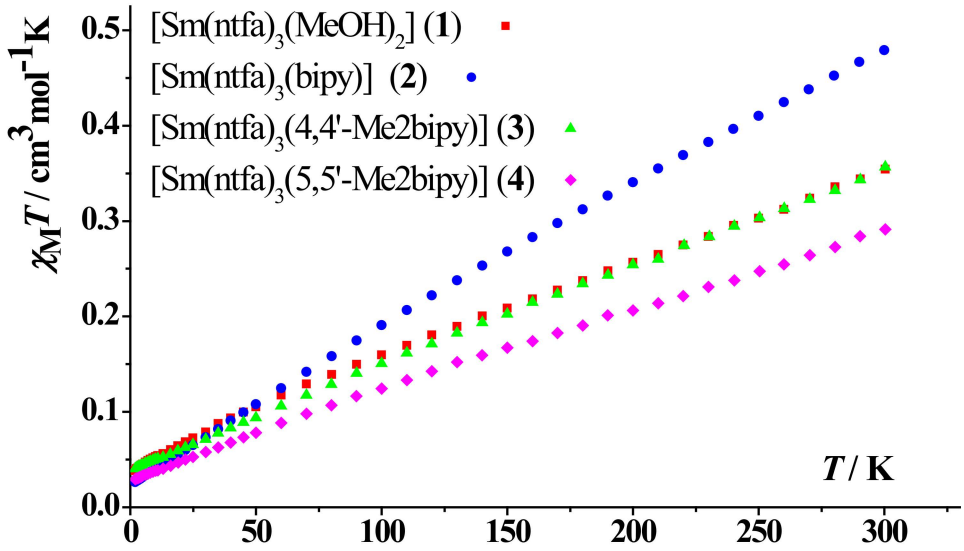

Figure 6. χ_MT vs. T plots for compounds **1**–**4**.

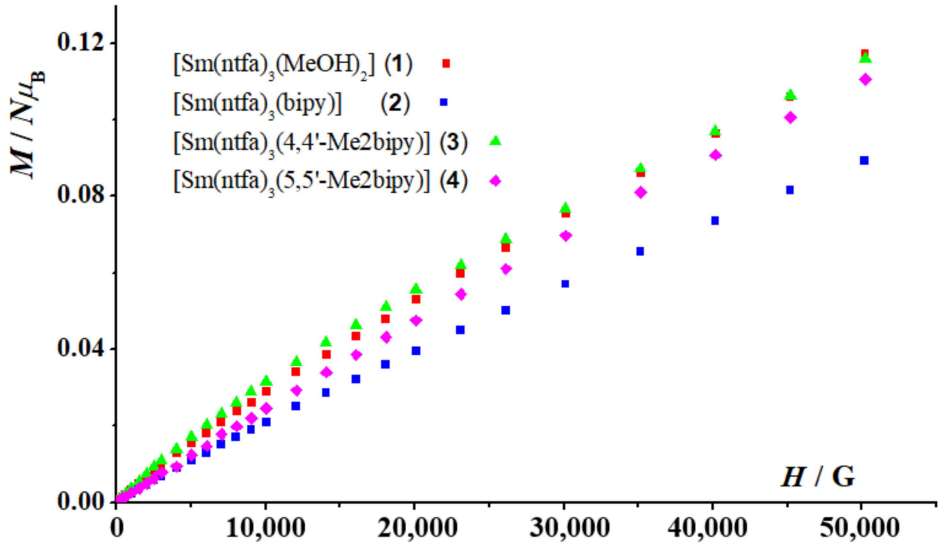

Figure 7. Magnetization plots measured at T = 2 K (field dependence of **1**–**4**).

Field dependence of the magnetization on the magnetic static applied field at T = 2 K for complexes **1**–**4** (Figure 7) revealed no saturation in high fields, with similar values of 0.12, 0.09, 0.12, and 0.11 $N\mu_B$ at 5 T for **1**–**4**, respectively. Taking into consideration the $4f^5$ ground configuration of the Sm(III) ion value, the saturated magnetization should have been 5/7 $N\mu_B$ (Msat = $g_J \cdot J \cdot N\mu_B$; g_J = 2/7, J = 5/2).

4. Conclusions

Similar to most of the Ln^{3+} ions, the reaction of an aqueous or alcoholic Ln(III) salts with β-diketonate ligands (ntfa = 4,4,4-trifluoro-1-(naphthalen-2-yl)-1,3-butanedionate; btfa = 4,4,4-trifluoro-1-phenyl-1,3-butanedionate; acac = acetylacetonate) in the presence of three equivalents of NaOH affords the tris β-diketonate complexes [Ln(β-diketonate)$_3$(Solv)$_2$] (Solv = H_2O, MeOH, EtOH) [29–33]. These compounds serve as precursors for the synthesis of many mononuclear polypyridyl adducts, with CNs varying between 8 in the cases of dipyridine derivatives such as phen, bipy, 4,4′-Me_2bipy, and 5,5′-Me_2bipy, and 9 in the case of terpy [26,27,29–33]. With no exception, four samarium(III) complexes [Sm(ntfa)$_3$(MeOH)$_2$] (**1**), [Sm(ntfa)$_3$(bipy)$_2$] (**2**), [Sm(ntfa)$_3$(4,4′-Me_2bipy)$_2$] (**3**), and [Sm(ntfa)$_3$(5,5′-Me_2bipy)$_2$] (**4**) were synthesized, and their single-crystal X-ray structures were determined. It has been reported that the use of auxiliary ligands with strong chelation properties enhanced the efficient transfer of energy in the visible and NIR regions, from the chelated pyridyl groups to the Ln^{3+} centers [29–32,38]. In addition, it was nearly established that combining aromatic rings and incorporation of fluorinated alkyl groups into the β-diketone skeletons significantly enhanced the emission luminescent of the resulting complexes [30–33,43–45,77]. Indeed, these two properties were included into the complexes **2**–**4**, which revealed luminescence emissions in the visible and NIR regions, a property that makes these compounds potential candidates in the light-devices field [12,62,73]. The magnetic investigation of the complexes **1**–**4** did not reveal any unusual magnetic behavior.

Supplementary Materials: The following supporting information can be downloaded at: https://www.mdpi.com/article/10.3390/magnetochemistry8070072/s1. CCDC 1964549–CCDC 1964553 contain the crystallographic data in CIF format for **1**–**4**, respectively. More Supplementary Materials corresponding to PXRD patterns are presented as Supplementary Figures S1–S4 and packing plots as Supplementary Figures S5–S8 for the four title complexes, respectively. Supplementary Tables S1–S4 contain C-H/F···ring and ring···ring noncovalent interactions for the four compounds, respectively. Absorption spectra (visible and UV region) of solid samples of **1**–**4** are represented in Supplementary Figure S9, and the deconvolution of the magnetic-dipole-allowed band $^4G_{5/2} \rightarrow {}^6H_{7/2}$ are shown in Supplementary Figure S10.

Author Contributions: Conceptualization, F.A.M., R.V. and S.S.M.; methodology, F.A.M., R.V., F.B., Á.T. and R.C.F.; software, F.A.M., R.C.F., F.B., S.S., Á.T. and R.V.; validation, F.A.M., R.V., R.C.F. and S.S.M.; investigation, F.B., Á.T., R.C.F. and S.S.; resources, F.A.M., R.C.F. and R.V.; data curation, F.A.M., F.B., R.C.F., S.S.; Á.T., R.V. and S.S.M.; writing and editing manuscript, F.A.M., S.S.M., Á.T. and R.V.; visualization, F.A.M., Á.T., R.V. and S.S.; administration of project and supervision, S.S.M., F.A.M. and R.V.; funding management, R.V.; The authors agree with the manuscript version presented. All authors have read and agreed to the published version of the manuscript.

Funding: Supported by TU Graz Open Access Publishing Fund. R.V. is thankful to MINECO for financial assistance (Project PGC2018-094031-B-I00).

Institutional Review Board Statement: Not applicable.

Informed Consent Statement: Not applicable.

Data Availability Statement: Data is contained within the article or Supplementary Materials.

Acknowledgments: R.V., S.S. and A.T. acknowledge the financial support from the Ministerio de Ciencia, Innovación y Universidades (Spain) under Project PGC2018-094031-B-100.

Conflicts of Interest: The authors declare no conflict of interest.

References

1. Wang, H.-S.; Zhao, B.; Zhai, B.; Shi, W.; Cheng, P.; Liao, D.-Z.; Yan, D.-Z. Syntheses, structures, and photoluminescence of one-dimensional lanthanide coordination polymers with 2,4,6-pyridinetricarboxylic acid. *Cryst. Growth Des.* **2007**, *7*, 1851. [CrossRef]
2. Melo, L.L.L.S.; Castro, G.P., Jr.; Gonçalves, S.M.C. Substantial intensification of the quantum Yield of samarium(III) complexes by mixing ligands: Microwave-assisted synthesis and luminescence Properties. *Inorg. Chem.* **2019**, *58*, 3265–3270. [CrossRef]
3. Cui, Y.; Yue, Y.; Qian, G.; Chen, B. Luminescent functional Metal–Organic Frameworks. *Chem. Rev.* **2012**, *112*, 1126–1162. [CrossRef] [PubMed]
4. Liu, W.; Li, Z.; Wang, N.; Li, X.; Wei, Z.; Yue, S.; Liu, Y. A new family of 3D heterometallic 3d–4f organodisulfonate complexes based on the linkages of 2D $[Ln(nds)(H_2O)]^+$ layers and $[Cu(ina)_2]^-$ chains. *Cryst. Eng. Comm.* **2011**, *13*, 138–144. [CrossRef]
5. Kelly, R.P.; Bell, T.D.M.; Cox, R.P.; Daniels, D.P.; Deacon, G.B.; Jaroschik, F.; Junk, P.C.; Le Goff, X.F.; Lemercier, G.; Martinez, A. Divalent tetra- penta-phenylcyclopentadienyl europium and samarium sandwich and half-sandwich complexes: Synthesis, characterization, and remarkable luminescence properties. *Organometallics* **2015**, *34*, 5624–5636. [CrossRef]
6. Bo, Q.-B.; Sun, G.-X.; Geng, D.-L. Novel Three-Dimensional Pillared-Layer Ln(III)−Cu(I) Coordination polymers featuring spindle-shaped heterometallic building units. *Inorg. Chem.* **2010**, *49*, 561–571. [CrossRef]
7. Feng, X.; Wang, L.-Y.; Zhao, J.-S.; Wang, J.-G.; Weng, N.S.; Liu, B.; Shi, X.-G. Series of anion-directed lanthanide-rigid-flexible frameworks: Syntheses, structures, luminescence, and magnetic properties. *Cryst. Eng. Comm.* **2010**, *12*, 774–783. [CrossRef]
8. Chandler, B.D.; Cramb, D.T.; Shimizu, G.K.H. Microporous metal−organic frameworks formed in a stepwise manner from luminescent building blocks. *J. Am. Chem. Soc.* **2006**, *128*, 10403–10412. [CrossRef]
9. Wu, Y.; Yang, J.; Lin, Y.; Xu, J. Synthesis of samarium-based metal organic compound nanoparticles with polychromatic-Photoluminescence for bio-tissue fluorescence Imaging. *Molecules* **2019**, *24*, 3657. [CrossRef]
10. Bui, A.T.; Grichine, A.; Brassele, S.; Duperray, A.; Andraud, C.; Maury, O. Unexpected efficiency of a luminescent samarium(III) complex for combined visible and near-infrared biphotonic microscopy. *Chem. Eur. J.* **2015**, *21*, 17757–17761. [CrossRef]
11. Knope, K.E.; de Lill, D.T.; Rowland, C.E.; Cantos, P.M.; de Bettencourt-Dias, A.; Cahill, C.L. Uranyl sensitization of samarium(III) luminescence in a two-dimensional coordination polymer. *Inorg. Chem.* **2012**, *51*, 201–206. [CrossRef] [PubMed]
12. Lunstroot, K.; Nockemann, P.; Van Hecke, K.; Van Meervelt, L.; Gorller-Walrand, C.; Binnemans, K.; Driesen, K. Visible and near-infrared emission by samarium(III)-containing ionic liquid mixtures. *Inorg. Chem.* **2009**, *48*, 3018–3026. [CrossRef]
13. Li, Z.; Yao, S.; Xu, J.; Wu, Y.; Li, C.; He, Z. Endoscopic near-infrared dental imaging with indocyanine green: A pilot study. *Ann. N. Y. Acad. Sci.* **2018**, *1421*, 88–96. [CrossRef] [PubMed]
14. Schaafsma, B.E.; Mieog, J.S.D.; Hutteman, M.; Van Der Vorst, J.R.; Kuppen, P.J.K.; Löwik, C.W.G.M.; Frangioni, J.V.; Van De Velde, C.J.H.; Vahrmeijer, A.L. The clinical use of indocyanine green as a near-infrared fluorescent contrast agent for image-guided oncologic surgery. *J. Surg. Oncol.* **2011**, *104*, 323–332. [CrossRef] [PubMed]
15. Troyan, S.L.; Kianzad, V.; Gibbs-Strauss, S.L.; Gioux, S.; Matsui, A.; Oketokoun, R.; Ngo, L.; Khamene, A.; Azar, F.; Frangioni, J.V. The FLARE intraoperative near-infrared fluorescence imaging system: A first-in-human clinical trial in breast cancer sentinel lymph node mapping. *Ann. Surg. Oncol.* **2009**, *16*, 2943–2952. [CrossRef]
16. Monteiro, J.H.S.K. Recent advances in luminescence imaging of biological systems using lanthanide(III) luminescent complexes. *Molecules* **2020**, *25*, 2089. [CrossRef] [PubMed]

17. Topa, M.; Ortyl, J.; Chachaj-Brekiesz, A.; Kamińska-Borek, I.; Maciej, P.; Popielarz, R. Applicability of samarium(III) complexes for the role of luminescent molecular sensors for monitoring progress of photopolymerization processes and control of the thickness of polymer coatings. *Spectrochim. Acta Part A Mol. Biomol. Spectrosc.* **2018**, *199*, 430–440. [CrossRef]
18. Chen, J.; Xie, Z.; Meng, L.; Hu, Z.; Kuang, X.; Xie, Y.; Lu, C.-Z. Luminescence tunable europium and samarium complexes: Reversible On/Off switching and white-light emission. *Inorg. Chem.* **2020**, *59*, 6963–6977. [CrossRef]
19. Philip, P.; Jose, T.; Jose, A.; Cherian, S.K. Studies on the structural and optical properties of samarium β-diketonate complex incorporated electrospun poly(methylmethacrylate) nanofibres with different architectures. *Luminescence* **2021**, *36*, 1032–1047. [CrossRef]
20. Mara, D.; Artizzu, F.; Laforce, B.; Vincze, L.; Van Hecke, K.; Van Deun, R.; Kaczmarek, A.M. Novel tetrakis lanthanide β-diketonate complexes: Structural study, luminescence properties and temperature sensing. *J. Lumin.* **2019**, *213*, 343–355. [CrossRef]
21. Bhat, S.A.; Iftikhar, K. Samarium complexes with fluorinated β-diketone and heterocyclic Lewis bases as UV light converters. *Dye. Pigment.* **2020**, *179*, 108383. [CrossRef]
22. Dar, W.A.; Ahmed, Z.; Iftikhar, K. Cool white light emission from the yellow and blue emission bands of the Dy(III) complex under UV excitation. *J. Photoch. Photobiol. A* **2018**, *356*, 502–511. [CrossRef]
23. Yao, X.; An, G.; Li, Y.; Yan, P.; Li, W.; Li, G. Effect of nuclearity and symmetry on the single-molecule magnets behaviour of seven-coordinated β-diketonate Dy(III) complexes. *J. Solid State Chem.* **2019**, *274*, 295–302. [CrossRef]
24. Li, X.; Li, T.; Tian, L.; Liu, Z.Y.; Wang, X.G. Experimental and theoretical interpretation of the magnetic behaviour of two Dy(III) single-ion magnets constructed through β-diketonate ligands with different substituent groups (–Cl/OCH_3). *RSC Adv.* **2015**, *5*, 74864–74873. [CrossRef]
25. Liu, C.-M.; Zhang, D.Q.; Zhu, D.-B. Field-induced single-ion magnets based on enantiopure chiral β-diketonate ligands. *Inorg. Chem.* **2013**, *52*, 8933–8940. [CrossRef]
26. Ansari, A.A.; Ganaie, A.B.; Iftikhar, K. Synthesis and 4f-4f absorption studies of tris(acetylacetonato) praseodymium(III) and holmium(III) complexes with imidazole and pyrazole in non-aqueous solvents. Structure elucidation by sparkle/PM7. *J. Mol. Struct.* **2019**, *1198*, 126826. [CrossRef]
27. Ansari, A.A.; Ilmi, R.; Iftikhar, K. Hypersensitivity in the 4f–4f absorption spectra of tris(acetylacetonato)neodymium(III) complexes with imidazole and pyrazole in non-aqueous solutions. Effect of environment on hypersensitive transitions. *J. Lumin.* **2012**, *132*, 51–60. [CrossRef]
28. Chen, G.-J.; Zhou, Y.; Jin, G.-X.; Dong, Y.-B. [$Dy(acac)_3(dppn)$]·C_2H_5OH: Construction of a single-ion magnet based on the square-antiprism dysprosium(III) ion. *Dalton Trans.* **2014**, *43*, 16659–16665. [CrossRef]
29. Mautner, F.A.; Bierbaumer, F.; Gyurkac, M.; Fischer, R.C.; Torvisco, A.; Massoud, S.S.; Vicente, R. Synthesis and characterization of lanthanum(III) complexes containing 4,4,4-trifluoro-1-(2-naphthalen-yl)-butane-1,3-dionate. *Polyhedron* **2020**, *179*, 114384. [CrossRef]
30. Mautner, F.A.; Bierbaumer, F.; Fischer, R.C.; Torvisco, A.; Vicente, R.; Font-Bardía, M.; Tubau, À.; Speed, S.; Massoud, S.S. Diverse coordination numbers and geometries in pyridyl adducts of lanthanide(III) complexes based on β-diketonate. *Inorganics* **2021**, *9*, 74. [CrossRef]
31. Mautner, F.A.; Bierbaumer, F.; Fischer, R.C.; Vicente, R.; Tubau, À.; Ferran, A.; Massoud, S.S. Structural characterization, magnetic and luminescent properties of praseodymium(III)-4,4,4-trifluoro-1-(2-naphthyl)butane-1,3-dionato(1-) complexes. *Crystals* **2021**, *11*, 179. [CrossRef]
32. Vicente, R.; Tubau, À.; Speed, S.; Mautner, F.A.; Bierbaumer, F.; Fischer, R.C.; Massoud, S.S. Slow magnetic relaxation and luminescence properties in neodymium(III)-4,4,4-trifluoro-1-(2-naphthyl)butane-1,3-dionato complexes incorporating bipyridyl ligands. *New J. Chem.* **2021**, *45*, 14713–14723. [CrossRef]
33. Mautner, F.A.; Bierbaumer, F.; Vicente, R.; Speed, S.; Tubau, A.; Font-Bardía, M.; Fischer, R.C.; Massoud, S.S. The luminescence and magnetic properties of 8-coordinated holmium(III)-trifluoro-phenyl- and naphthalenyl-β-diketonate complexes. *Molecules* **2022**, *27*, 1129. [CrossRef] [PubMed]
34. Casanovas, B.; Speed, S.; Maury, O.; Font-Bardía, M.; Vicente, R. Homodinuclear lanthanide 9-anthracenecarboxylate complexes: Field induced SMM and NIR-luminescence. *Polyhedron* **2019**, *169*, 187–194. [CrossRef]
35. Ansari, A.A.; Hussain, H.A.; Iftikhar, K. Optical absorption spectroscopic studies on holmium(III) complexes with β-diketone and heterocyclic amines. The environment effect on 4f–4f hypersensitive transitions. *Spectrochim. Acta Part A* **2007**, *68*, 1305–1312. [CrossRef]
36. Ansari, A.A.; Ahmed, Z.; Iftikhar, K. Nuclear magnetic resonance and optical absorption spectroscopic studies on paramagnetic praseodymium(III) complexes with β-diketone and heterocyclic amines. *Spectrochim. Acta Part A* **2007**, *68*, 176–183. [CrossRef]
37. Chauhan, A.; Langyan, R. Photosensitization in highly luminescent nonmacrocyclic samarium(III) complexes for application in light-emitting systems. *J. Photochem. Photobiol. A Chem.* **2022**, *424*, 113627. [CrossRef]
38. Bünzli, J.-C.G. On the design of highly luminescent lanthanide complexes. *Coord. Chem. Rev.* **2015**, *293*, 19–47. [CrossRef]
39. Jia, J.-H.; Li, Q.-W.; Chen, Y.-C.; Liu, J.-L.; Tong, M.-L. Luminescent single-molecule magnets based on lanthanides: Design strategies, recent advances and magneto-luminescent studies. *Coord. Chem. Rev.* **2019**, *378*, 365–381. [CrossRef]
40. Armelao, L.; Quici, S.; Barigelletti, F.; Accorsi, G.; Bottaro, G.; Cavazzini, M.; Tondello, E. Design of luminescent lanthanide complexes: From molecules to highly efficient photo-emitting materials. *Coord. Chem. Rev.* **2010**, *254*, 487–505. [CrossRef]

41. Quici, S.; Cavazzini, M.; Marzanni, G.; Accorsi, G.; Armaroli, N.; Ventura, B.; Barigelletti, F. Visible and near-infrared intense luminescence from water-soluble lanthanide [Tb(III), Eu(III), Sm(III), Dy(III), Pr(III), Ho(III), Yb(III), Nd(III), Er(III)] complexes. *Inorg. Chem.* **2005**, *44*, 529–537. [CrossRef] [PubMed]
42. Bünzli, J.-C.G.; Piguet, C. Taking advantage of luminescent lanthanide ions. *Chem. Soc. Rev.* **2005**, *34*, 1048–1077. [CrossRef] [PubMed]
43. Tu, H.-R.; Sun, W.-B.; Li, H.-F.; Chen, P.; Tian, Y.-M.; Zhang, W.-Y.; Zhang, Y.-Q.; Yan, P.-F. Complementation and joint contribution of appropriate intramolecular coupling and local ion symmetry to improve magnetic relaxation in a series of dinuclear Dy2 single-molecule magnets. *Inorg. Chem. Front.* **2017**, *4*, 499–508. [CrossRef]
44. Dasari, S.; Singh, S.; Sivakumar, S.; Patra, A.K. Dual-Sensitized luminescent europium(III) and terbium(III) complexes as bioimaging and light-responsive therapeutic agents. *Chem.-Eur. J.* **2016**, *22*, 17387–17396. [CrossRef] [PubMed]
45. Bruno, S.M.; Ananias, D.; Paz, F.A.A.; Pillinger, M.; Valente, A.A.; Carlos, L.D.; Goncalves, I.S. Crystal structure and temperature-dependent luminescence of a heterotetranuclear sodium–europium (III) β-diketonate complex. *Dalton Trans.* **2015**, *44*, 488–492. [CrossRef]
46. Zhang, S.; Ke, H.; Shi, Q.; Zhang, J.; Yang, Q.; Wei, Q.; Xie, G.; Wang, W.; Yang, D.; Chen, S. Dysprosium(iii) complexes with a square-antiprism configuration featuring mononuclear single-molecule magnetic behaviours based on different β-diketonate ligands and auxiliary ligands. *Dalton Trans.* **2016**, *45*, 5310–5320. [CrossRef]
47. Trieu, T.-N.; Dinh, T.-H.; Nguyen, H.-H.; Abram, U.; Nguyen, M.-H. Novel lanthanide (III) ternary complexes with naphthoyltrifluoroacetone: A synthetic and spectroscopic study. *Z. Anorg. Allg. Chem.* **2015**, *641*, 1934–1940. [CrossRef]
48. Hasegawa, Y.; Nakagawa, Y.; Kawai, T. Recent progress of luminescent metal complexes with photochromic units. *Coord. Chem. Rev.* **2010**, *254*, 2643–2651. [CrossRef]
49. Maggini, I.; Traboulsi, H.; Yoosaf, K.; Mohanraj, J.; Wouters, J.; Pietraszkiewicz, O.; Pietraszkiewicz, M.; Armaroli, N.; Bonifazi, D. Electrostatically-driven assembly of MWCNTs with a europium complex. *Chem. Commun.* **2011**, *47*, 1625–1627. [CrossRef]
50. Marin, R.; Brunet, G.; Murugesu, M. Shining new light on multifunctional lanthanide single-molecule magnets. *Angew. Chem.* **2019**, *60*, 1728–1746. [CrossRef]
51. Vancaeyzeele, C.; Ornatsky, O.; Baranov, V.; Shen, L.; Abdelrahman, A.; Mitchell, A.; Winnik, M.A. Lanthanide-containing polymer nanoparticles for biological tagging applications: Nonspecific endocytosis and cell adhesion. *J. Am. Chem. Soc.* **2007**, *129*, 13653–13660. [CrossRef] [PubMed]
52. Degen, T.; Sadki, M.; Bron, E.; König, U.; Nenert, G. The HighScore suite. *Powder Diffr.* **2014**, *29*, S13–S18. [CrossRef]
53. Bain, G.A.; Berry, J.F. Diamagnetic corrections and Pascal's constants. *J. Chem. Educ.* **2008**, *85*, 532–536. [CrossRef]
54. Bruker. *APEX, SAINT v. 8.37A*; Bruker AXS Inc.: Madison, WI, USA, 2015.
55. Sheldrick, G.M. *SADABS v. 2*; University of Goettingen: Goettingen, Germany, 2001.
56. Sheldrick, G.M. Crystal structure refinement with SHELXL. *Acta Crystallogr. C Struct. Chem.* **2015**, *71*, 3–8. [CrossRef]
57. Sheldrick, G.M. A Short history of SHELX. *Acta Crystallogr. A* **2008**, *64*, 112–122. [CrossRef]
58. Macrae, C.F.; Edington, P.R.; McCabe, P.; Pidcock, E.; Shields, G.P.; Taylor, R.; Towler, T.; van de Streek, J.J. Mercury: Visualization and analysis of crystal structures. *Appl. Cryst.* **2006**, *39*, 453–457. [CrossRef]
59. Spek, A.L. *Platon, a Multipurpose Crystallographic Tool*; Utrecht University: Utrecht, The Netherlands, 1999.
60. Alvarez, S.; Alemany, P.; Casanova, D.; Cirera, J.; Llunell, M.; Avnir, D. Shape maps and polyhedral interconversion paths in transition metal chemistry. *Coord. Chem. Rev.* **2005**, *249*, 1693–1708. [CrossRef]
61. Cirera, J.; Alvarez, S. Stereospinomers of pentacoordinate iron porphyrin complexes: The case of the [Fe(porphyrinato)(CN)]$^{-}$ anions. *Dalton. Trans.* **2013**, *42*, 7002–7008. [CrossRef]
62. Foucault-Collet, A.; Shade, C.M.; Nazarenko, I.; Petoud, S.; Eliseeva, S.V. Polynuclear Sm(III) polyamidoamine-based dendrimer: A single probe for combined visible and near-infrared live-cell imaging. *Angew. Chem. Int. Ed. Engl.* **2014**, *53*, 2927–2930. [CrossRef]
63. Bolton, J. New NIR emission from Sm^{3+} in Yb^{3+}-Sm^{3+} co-doped tellurite glass. *J. Lumin.* **2021**, *231*, 117717. [CrossRef]
64. Biju, S.; Eom, Y.K.; Bünzli, J.C.G.; Kim, H.K. A new tetrakis β-diketone ligand for NIR emitting Ln III ions: Luminescent doped PMMA films and flexible resins for advanced photonic applications. *J. Mater. Chem. C* **2013**, *1*, 6935–6944. [CrossRef]
65. Brito, H.F.; Malta, O.L.; Felinto, M.C.F.C.; Teotonio, E.E.S.; Menezes, J.F.S.; Silva, C.F.B.; Tomiyama, C.S.; Carvalho, C.A.A. Luminescence investigation of the Sm(III)-β-diketonates with sulfoxides, phosphine oxides and amides ligands. *J. Alloy. Compd.* **2002**, *344*, 293–297. [CrossRef]
66. De Bettencourt-Dias, A. (Ed.) *Luminescence of Lanthanide Ions in Coordination Compounds and Nanomaterials*; John Wiley & Sons Ltd.: Hoboken, NJ, USA, 2014.
67. Kahn, O. *Molecular Magnetism*; VCH Publishers: Hoboken, NJ, USA, 1993.
68. Chi, Y.-X.; Niu, S.-Y.; Jin, J. Syntheses, structures and photophysical properties of a series of Zn–Ln coordination polymers (Ln = Nd, Pr, Sm, Eu, Tb, Dy). *Inorg. Chim. Acta* **2009**, *362*, 3821–3828. [CrossRef]
69. Yuan, B.; Wang, F.; Tao, J.; Li, M.; Yang, X. Self-assembly of one visible and NIR luminescent Sm(III) coordination polymer with flexible Schiff base ligand. *Inorg. Chim. Acta* **2019**, *490*, 24–28. [CrossRef]
70. Sun, L.-N.; Yu, J.-B.; Zhang, H.-J.; Meng, Q.-G.; Ma, E.; Peng, C.-Y.; Yang, K.-Y. Near-infrared luminescent mesoporous materials covalently bonded with ternary lanthanide [Er(III), Nd(III), Yb(III), Sm(III), Pr(III)] complexes. *Microporous Mesoporous Mater.* **2007**, *98*, 156–165. [CrossRef]

71. Chauhan, A.; Langyan, R. Preparation, characterization and luminescence behaviour of some samarium complexes. *Rare Met.* **2021**, *40*, 2618–2626. [CrossRef]
72. Gonçalves e Silva, F.R.; Malta, O.L.; Reinhard, C.; Güdel, H.-U.; Piguet, C.; Jacques, E.; Moser, J.E.; Jean-Claude, G.; Bünzli, J.-C.G. Visible and near-infrared luminescence of lanthanide-containing dimetallic triple-stranded helicates: Energy transfer mechanisms in the SmIII and YbIII molecular edifices. *J. Phys. Chem. A* **2002**, *106*, 1670–1677. [CrossRef]
73. Bassett, A.P.; Magennis, S.W.; Glover, P.B.; Lewis, D.J.; Spencer, N.; Parsons, S.; Williams, R.M.; De Cola, L.; Pikramenou, Z. Highly luminescent, triple- and quadruple-stranded, dinuclear Eu, Nd, and Sm(III) lanthanide complexes based on bis-diketonate ligands. *J. Am. Chem. Soc.* **2004**, *126*, 9413–9424. [CrossRef]
74. Wang, S.; Xu, J.; Wang, J.; Wang, K.-Y.; Dang, S.; Song, S.; Liu, D.; Cheng, W. Luminescence of samarium(III) bis-dithiocarbamate frameworks: Codoped lanthanide emitters that cover visible and near-infrared domains. *J. Mater. Chem. C* **2017**, *5*, 6620–6628. [CrossRef]
75. Atwood, D.A. (Ed.) *The Rare Earth Elements: Fundamentals and Applications*; John Wiley & Sons Ltd.: Hoboken, NJ, USA, 2005.
76. Wu, A.Q.; Zheng, F.-K.; Liu, X.; Guo, G.-C.; Cai, L.-Z.; Dong, Z.-C.; Takano, Y.; Huang, J.-S. A novel bi-layered samarium complex with an unprecedented coordination mode of orotic acid $[Sm_2(HL)_2(ox)(H_2O)_2]_n \cdot 2.5nH_2O$ (H_3L = orotic acid, ox^{2-} = oxalate^{2-}): Synthesis, crystal structure and physical properties. *Inorg. Chem. Commun.* **2006**, *9*, 347–350. [CrossRef]
77. Andruh, M.; Bakalbassis, E.; Kahn, O.; Trombe, J.C.; Porcher, P. Structure, spectroscopic and magnetic properties of rare earth metal (III) derivatives with the 2-formyl-4-methyl-6-(N-(2-pyridylethyl)(formimidoyl) phenol ligand. *Inorg. Chem.* **1993**, *32*, 1616–1622. [CrossRef]
78. Pan, Y.-Z.; Hua, Q.-Y.; Lin, L.-S.; Qiu, Y.-B.; Liu, J.-L.; Zhou, A.-J.; Lin, W.-Q.; Leng, J.-D. A slowly magnetic relaxing Sm^{III} monomer with a D_{5h} equatorial compressed ligand field. *Inorg. Chem. Front.* **2020**, *7*, 2335–2342. [CrossRef]